Composites: Part B 54 (2013) 353–364

Contents lists available at SciVerse ScienceDirect

Composites: Part B

journal homepage: www.elsevier.com/locate/compositesb

Molecular modeling of crosslinked graphene–epoxy nanocomposites for characterization of elastic constants and interfacial properties

R. Rahman [a,*], A. Haque [b]

[a] Center for Simulation, Visualization and Real-Time Prediction (SiViRt), The University of Texas at San Antonio, TX 78249, United States
[b] The Department of Aerospace Engineering & Mechanics, The University of Alabama, Tuscaloosa, AL 35487, United States

ARTICLE INFO

Article history:
Received 3 August 2012
Received in revised form 14 March 2013
Accepted 26 May 2013
Available online 5 June 2013

Keywords:
A. Nano-structures
B. Mechanical properties
B. Elasticity
C. Computational modeling

ABSTRACT

The mechanical properties of crosslinked graphene/epoxy nanocomposites have been investigated using molecular mechanics (MM) and molecular dynamics simulations (MD). The influence of graphene nanoplatelet concentrations, aspect ratios and dispersion on elastic constants and stress–strain responses are studied. The cohesive and pullout forces at the interface of G–Ep nanocomposites are also investigated. The simulated MD models were further analyzed through radial distribution function, molecular energy and atom density. The results show significant improvement in Young's modulus and shear modulus for the G–Ep system in comparison to neat epoxy resin. The graphene concentrations in the range of 1–3% and graphene with low aspect ratio are seen to improve Young's modulus. The dispersed graphene system is seen to enhance in-plane elastic modulus than the agglomerated graphene system. The cohesive and pullout forces versus displacements data were plotted under normal and shear modes in order to characterize interfacial properties. The cohesive force is significantly improved by attaching chemical bonding at the graphene–epoxy interface. It appears that elastic constants determined by molecular modeling and nanoindentation test methods are comparatively higher than the micromechanics based predicted value and coupon test data. This is possibly due to scaling effect.

1. Introduction

Epoxy resin exhibits excellent mechanical properties such as high elastic modulus and fracture strength, low creep and less environmental degradation which made it attractive candidate for coatings, adhesives and resin for structural composites particularly in aerospace and electronic industries. It has been reported that the structural properties of neat epoxy resins may be improved by reinforcing them with carbon nanotubes (CNT), nanoclays (NC) and graphene nanoplatelets (GNP), and carbon nanofibers (CNF) [1–6]. But most of the earlier studies related to epoxy based nanocomposites are primarily experimental which lacks sufficient physical understanding about the interactions of nanomaterials with neat resin particularly in terms of their concentration, aspect ratios and dispersion. The effects of these parameters in the overall optimum mechanical properties of nanocomposites are significantly important. Furthermore, the stress transfer at the interface of nanomaterials and neat resin is another critical factor which also controls the mechanical properties of nanocomposites. As a result both experimental as well as theoretical studies of epoxy based nanocomposites are emphasized in order to achieve optimum benefits. The theoretical study of epoxy based nanocomposites has been carried out at continuum scale using analytical and finite element method [7]. However, continuum level analysis omits detail structural configuration of nanomaterials at the molecular level and lacks true realistic interactions at the nanoscales. This limits the continuum scale study inadequate at certain stage when detail structural, thermodynamic or interfacial properties are required. It appears that molecular modeling is an effective theoretical tool in understanding the properties of nanocomposites [8].

Wu and Xu [9] performed MD simulation of cross-linked Diglycidyl Ether Bisphenol A (DGEBA) epoxy with isophorone diamine (IPD) curing agent and determined elastic constants, unit cell dimension and density. Fan and Yuen [10] also carried out MD simulation for cross-linked Diglycidyl Ether Bisphenol F (EPON 862) epoxy in presence of the curing agent Triethylenetetramine (TETA). They outlined MD simulation methodology in detail and determined Young's modulus, glass transition temperature of the cross-linked epoxy network. Recently, Bandyopadhay et al. [11] studied the mechanical and thermal properties of cross-linked epoxy polymer using atomistic modeling. In last few years scientists are more interested in studying mechanical properties of crosslinked epoxy resin reinforced with nanomaterials using MD simulation. In this context, Yu and others [12] performed a MD analysis of epoxy (EPON 862)/alumina (Al_2O_3) nanocomposites. Their study showed that the mechanical property is improved due to added alumina nanofillers

* Corresponding author. Tel.: +1 2052390559.
E-mail address: rezwanrehman@gmail.com (R. Rahman).

1359-8368/$ - see front matter © 2013 Elsevier Ltd. All rights reserved.
http://dx.doi.org/10.1016/j.compositesb.2013.05.034

in the epoxy matrix. Zhu and coworkers [8] predicted the stress–strain behavior of single walled carbon nanotube (SWNT) reinforced epoxy nanocomposites using molecular dynamics (MD) simulation scheme. Frankland and co-researchers [13] investigated the effect of polymer–nanotube cross-linking on critical load transfer mechanism from carbon nanotubes to polymer matrix using molecular dynamics (MD) simulation. Using MD simulation as well as micromechanics methods Choi et al. [14] performed a multiscale modeling of epoxy/silica nanocomposite. Yang et al. [15,16] also performed multiscale analysis of polyimide/silica systems using MD and micromechanics based model. Their study showed that introducing nanoparticles in the polymer matrix composites can enhance the mechanical as well as thermal properties.

Besides alumina, silica or CNT, graphene platelet (GNP) has drawn attention as filler/reinforcing material to enhance the mechanical, electrical and thermal property of traditional polymer system [4]. It is to be noted that GNPs are comparatively less expensive than CNT and they posses very high stiffness. This makes GNPs as an attractive candidate for filler materials in polymer nanocomposites. Cho and co-workers [5] predicted the elastic constants of graphite using molecular mechanics model and subsequently determined the elastic constants of graphite/epoxy nanocomposites using micromechanical model based on Mori–Tanaka method. Rafiee and co-researchers studied the enhancement of mechanical properties of graphene–epoxy nanocomposites in presence of low graphene content [6]. Yasmine and Daniel determined experimentally thermal properties and elastic modulus of graphite/epoxy nanocomposites [4]. Xiang and coworkers [17] developed a micromechanics model for graphene–polymer nanocomposite based on Mori–Tanaka model. It appears that the MD simulation work can be remarkably useful in addressing the influence of weight concentrations, aspect ratios and dispersion on elastic constants of GNP/epoxy nanocomposites.

Recently, it has been observed that the improved mechanical properties of the polymer composites not only depends on the inherent properties of the nanofiller, but also more importantly depends on interface energy and nanoscale morphology within the polymer matrix [18]. In last few years several researchers have focused on studying interfacial bonding between CNT and polymer matrix materials [7,8,19]. In these works the pullout strength, critical length of CNT in matrix and stress transfer at the CNT/epoxy interface etc. have been investigated. Aswathi [20] analyzed pullout as well as cohesive interaction in graphene–polyethylene system using molecular dynamics (MD) simulation. This cohesive interaction between a nanofiller surface and polymer is usually controlled by the van der Waals energy. However, both the pullout (shear) and cohesive strength (normal) of graphene in epoxy resin are important parameters which require further attention.

In this study, the effects of GNP weight concentration, aspect ratio and dispersion on stress–strain response and elastic constants are investigated using molecular modeling. The molecular simulation results are compared with available experimental data and predictions by micromechanics model.

2. Theory

MD uses Newton's equation of motion in defining the trajectory of atoms in any system. The forces on atoms are computed at each time interval and then combined with existing position and velocity to update them for next time step. In this work *pcff* force field is used to specify the molecular interactions in all the graphene–epoxy systems [10,21]. *pcff* force field consists of bonded energy terms, cross-terms and non-bonded energy terms. The bonded energy terms consist of bond stretch, angle bending and dihedral angle rotation energies. The cross interaction terms come from dynamic vibrations among bond stretch; angle bending and dihedral rotation. The non-bonded energy terms refer to energy due to Columbic and van der Walls interactions. Columbic interaction was applied using Ewald summation technique.

2.1. Atomistic stress calculation

The total energy in a system is based on contribution from both kinetic and potential energies. Hence the Hamiltonian based on this kinetic and potential part of total energy leads to calculate stress tensor σ_{ij} per Ith atom, (both tensile and compressive) is obtained from the following *virial* expression [5].

$$\sigma_{ij} = -\frac{1}{Vol}\left[\left(\sum_{I=1}^{N} m_I\left(v_i^I v_i^{I^T}\right)\right) + \left(\sum_{I<J} r_{ij}^{IJ} f_{ij}^{IJ^T}\right)\right] \tag{1}$$

where Vol is the volume of the simulation box, m_I is mass of Ith atom, v_i^I is the velocity of Ith atom in ith direction, N is total number of atoms, r_{ij}^{IJ} is ij-component of the distance between Ith and Jth atoms, f_{ij}^{IJ} is ij-component of the force between Ith and Jth atoms.

2.2. Elastic modulus using MM method

The elastic constants of a polymer system can be determined by using several methods. In MM method, the elastic constants were determined from the changes in total potential energy subjected to uniaxial deformation of the structures ignoring the kinetic energy due to molecular motion. The amorphous cell model undergoes extension and compression in order to determine elastic properties. It is reported by Theodorou and Suter [17] that the entropic contribution to an elastic response can be neglected in polymeric glasses. As a result the first term with velocity components in Eq. (1) is not considered in MM simulation. The first derivative of the potential energy with respect to strain provides internal stress tensor and the second derivative represents stiffness matrix. The unit cell (simulation box) undergoes unidirectional tensile and compressive deformations in all direction, $\boldsymbol{\varepsilon} = [\varepsilon_{11} \quad \varepsilon_{22} \quad \varepsilon_{33} \quad \varepsilon_{44} \quad \varepsilon_{55} \quad \varepsilon_{66}]$. Thus, the corresponding stresses in the system (σ_i^+ and σ_i^-) are calculated using Eq. (1). Hence, the stiffness components can be written in terms of stress components as [22].

$$C_{ij} = \frac{\sigma_i^+ - \sigma_i^-}{2\Delta\varepsilon_j} \tag{2}$$

The deformation process is considered to be strain controlled. In Eq. (1), σ_i is the ith component of internal stress tensor and σ_i^+, σ_i^- correspond to stress component under tension and compression. The change in strain components $\Delta\varepsilon_j$ is $2\varepsilon_j$ due to tensile and compressive deformation. The entire stiffness matrix can be calculated using Eq. (2). Assuming ideal isotropic condition, Lame's constants λ, μ were calculated using Eq. (3). So, the Young's modulus and shear modulus of the system can be calculated using the following equations [22]:

$$\begin{aligned} &E = \mu\tfrac{3\lambda+2\mu}{\lambda+\mu} \quad \text{Young's modulus} \\ &G = \mu \quad \text{Shear modulus} \\ &\lambda = \tfrac{1}{3}(C_{11}+C_{22}+C_{33}) - \tfrac{2}{3}(C_{44}+C_{55}+C_{66}) \\ &\mu = \tfrac{1}{3}(C_{44}+C_{55}+C_{66}) \end{aligned} \tag{3}$$

2.3. Stress–strain responses using MD method

Besides computing the elastic properties using MM method, it is also possible to obtain stress–strain relationship using MD simulation. The purpose is to perform numerical experiments with the unit cell by applying uniaxial deformation. In general, any uniaxial deformation causes atoms in the system to move along the applied strain. The stress can be represented as an average of all the

principle stresses or "hydrostatic stress". So, for any small applied strain ε, the average stress in the system is calculated using Eq. (4). Each stress component is calculated from the virial stress expression in Eq. (1) without ignoring the dynamic motion of the molecules

$$\bar{\sigma} = \frac{(\sigma_{11} + \sigma_{22} + \sigma_{33})}{3} \tag{4}$$

where $\sigma_{11}, \sigma_{22}, \sigma_{33}$ virial stress in axial directions, $\bar{\sigma}$ is the hydrostatic stress. After every applied deformation the running averaged hydrostatic stress $\bar{\sigma}$ is calculated in order to smoothen the stress–strain response. The Young's modulus is also obtained from the slope of the linear regime of the stress–strain curve.

3. Model development

3.1. Amorphous model

The molecular model of amorphous crosslinked graphene–epoxy (G–Ep) nanocomposite system is developed in order to study the effects of graphene concentrations and aspect ratios on mechanical properties such as stress–strain responses, Young's modulus and shear modulus. The model is also implied in investigating some important structural parameters such as radial distribution function (RDF), atom density, and molecular energy pertinent to G–Ep system. A typical amorphous cross-linked epoxy unit cell contains epoxy and curing agent in the ratio of 12:4 [10]. During cross-linking process, reactive sites from EPON 862 (epoxide groups) create new bonds with reactive sites from TETA (sites containing NH and NH_2). If they come close enough to each other within range of 4–10 Å [12], the cross-linking occurs. Cross-linking process between EPON 862 and TETA is non-trivial. The computational cost becomes higher as the number of EPON 862 and TETA molecules increases. Hence, Yu and coauthors proposed to use a *representative cross-linked epoxy unit* composed of three EPON 862 molecules and one TETA molecule with cross-link ratio of 0.5 [12]. In this representative unit, three reactive sites of TETA are connected to three EPON molecules. This is schematically shown in Fig. 1(left). Each unit consists of 157 atoms. Yu and coauthors concluded that, the mechanical properties of cross-linked epoxy comprising of this representative epoxy unit showed reasonable agreement with experimental observations. So, keeping the similar idea in mind, this representative cross-linked unit was used in the current work. The initial representative molecule was constructed using open source molecular modeling software XENOVIEW [24] with pcff forcefield. Afterwards, an in-house code was developed to replicate this representative epoxy molecule in multiple numbers of times along with graphene sheets to construct graphene–epoxy amorphous unitcells. Graphene sheet is a 2D nanostructure consists of carbon atoms bonded by sp^2 hybridized electrons. The carbon atoms are arranged in a hexagonal pattern with the shortest distance of 1.42 Å between atoms with bond angle 120°. Single layer graphene possesses very high mechanical properties. The average Young's modulus of single layer zigzag graphene sheet with length 20.18 nm and width 4.18 nm is 1.033 TPa [25]. In this study graphene sheets with two different sizes were considered. These were defined in terms of aspect ratios AR-LW or AR-LT. AR-LW is length to width ratio and AR-LT is length to thickness ratio. Based on aspect ratio, the graphene sheets are named as Type-a: AR-LW $\geqslant$ 5.0, AR-LT $\geqslant$ 150 and Type-b: AR-LW $\geqslant$ 10.0 and AR-LT $\geqslant$ 480. The graphene sheets with hydrogen terminated edges were embedded in 3D periodic amorphous unit cells for evaluating elastic properties. Molecular model of these two types of graphene sheets were also constructed using XENOVIEW with pcff forcefield.

In this study 1%, 3% and 5% of graphene by weight was considered in the amorphous unit cell. The initial density of amorphous graphene–epoxy unit cells was kept in the range of 1.0 gm/cc. Using initial density, the initial dimension of each unitcell was estimated. The number of epoxy monomers was determined in such a way that it ensures expected weight percentage of graphene in the unit cell. Each unitcell consists of one graphene and randomly positioned multiple number of representative epoxy molecules based on a graphene's concentration. Final configuration of each unitcell was obtained by equilibrating the model using MD. Table 1 shows unitcell configurations with relevant graphene aspect ratios and weight percentages. Fig. 1 schematically describes the development of amorphous unitcell consisting of single graphene and multiple numbers of representative cross-liked epoxy units.

3.2. Stacked graphene model

The effects of single, dispersed and agglomerated graphenes on stress–strain responses and Young's modulus were studied using stacked graphene model (SGM). The SGM of graphene–epoxy nanocomposite consisting of single graphene, dispersed and agglomerated layered graphenes were developed as shown in Fig. 2. The unit cell configurations of three stacked graphene models are listed in Table 2. Each unitcell consists of less than 3% graphene with symmetry P3m [26]. Average graphene–epoxy

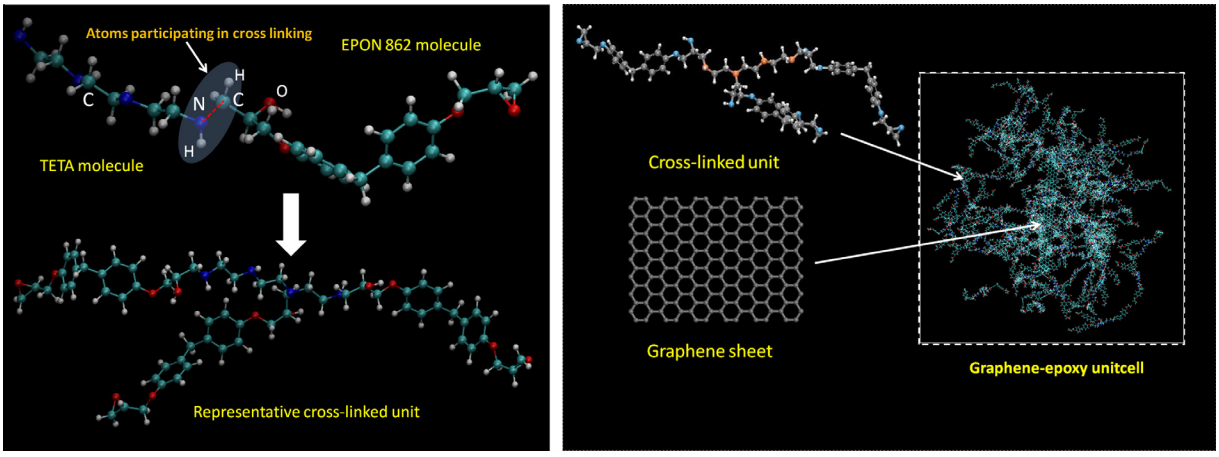

Fig. 1. Schematic diagram of developing amorphous model for graphene–epoxy system.

Table 1
Material configurations of G–Ep amorphous system.

Material configuration	Aspect ratio (AR)	Weight percentage of graphene (%)	Unit cell dimension (Å)	Number of representative epoxy molecules
G–Ep-Nc-I	AR-LW ⩾ 5, AR-LT ⩾ 150 (Type-a)	1	$a = b = c = 65$	70
G–Ep-Nc-II	AR-LW ⩾ 10, AR-LT ⩾ 480 (Type-b)	1	$a = b = c = 90$	280
G–Ep-Nc-III	AR-LW ⩾ 5, AR-LT ⩾ 150 (Type-a)	3	$a = b = c = 38.8$	22
G–Ep-Nc-IV	AR-LW ⩾ 10, AR-LT ⩾ 480 (Type-b)	3	$a = b = c = 62$	90
G–Ep-Nc-V	AR-LW ⩾ 5, AR-LT ⩾ 150 (Type-a)	5	$a = b = c = 33$	13
G–Ep-Nc-VI	AR-LW ⩾ 10, AR-LT ⩾ 480 (Type-b)	5	$a = b = c = 52.3$	53

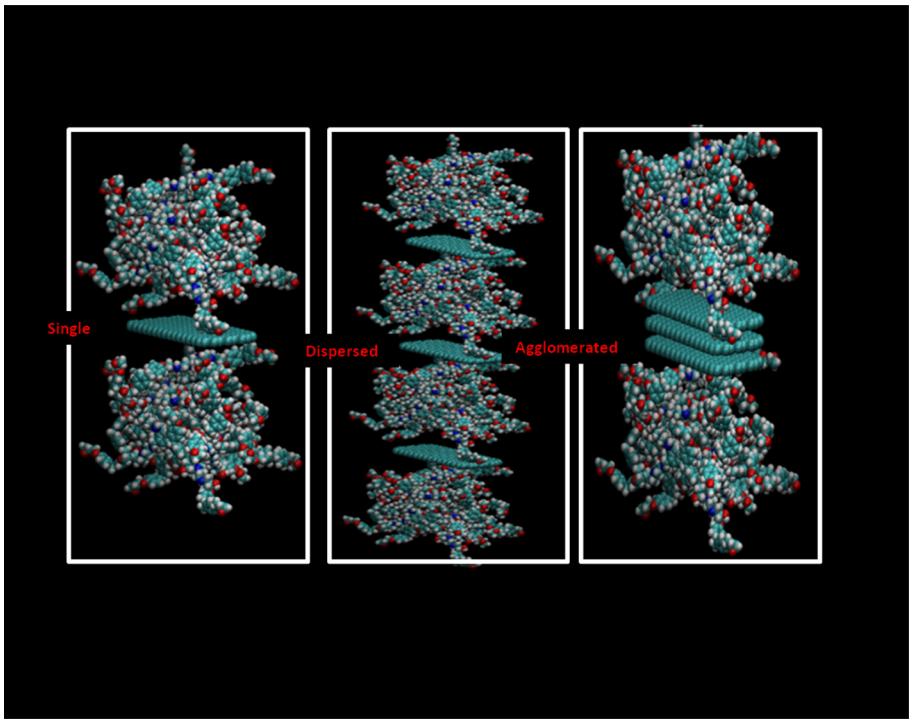

Fig. 2. Schematic diagram of stacked graphene model (SGM).

Table 2
Material configurations of SGM-G–Ep system.

Configuration	Unit cell dimension (Å)	Number of graphene plates	Number of representative epoxy molecules
SGM-G–Ep-I	$a = 9.84$, $b = 19.02$, $c = 1056.42$	1	46
SGM-G–Ep-II	$a = 9.84$, $b = 19.02$, $c = 2116.24$	3 (Dispersed)	68
SGM-G–Ep-III	$a = 9.84$, $b = 19.02$, $c = 3104.21$	3 (Agglomerated)	68

spacing is seen to be approximately 2 Å. The fundamental difference between amorphous and stacked graphene models is the local periodicity of graphene platelets.

3.3. Interface model

Molecular model calculates total potential energy of a N-atoms system. This leads to calculating force on each atom as force is negative of gradient of the energy. It is possible to evaluate interaction between a polymer and nanostructure at atomic scale. The interactions can be determined in couple of ways. One is by evaluating normal separation force $F_{Cohesive}$ and another is by evaluating shear separation force $F_{Pullout}$. These forces are calculated from the change in interaction energy between the nanostructure and polymer system. Once the nanofiller is moved away from the polymer matrix it experiences reaction forces either $F_{Cohesive}$ or $F_{Pullout}$ based on the direction of nanofiller movement. The system is non-periodic along the direction of displacement [23]. The interface models as shown in Fig. 3 were developed in order to study the load transfer mechanism between graphene and epoxy matrix. Graphenes with two different lengths (39.36 Å and 118.08 Å) were considered in order to evaluate the effect of aspect ratio. Both normal (mode-I) and shear separations (mode-II) were considered. For normal mode separation, epoxy molecules reside above a single graphene sheet whereas in shear separation, epoxy molecules reside on both side of the graphene sheet. Graphene is free to move in z-direction

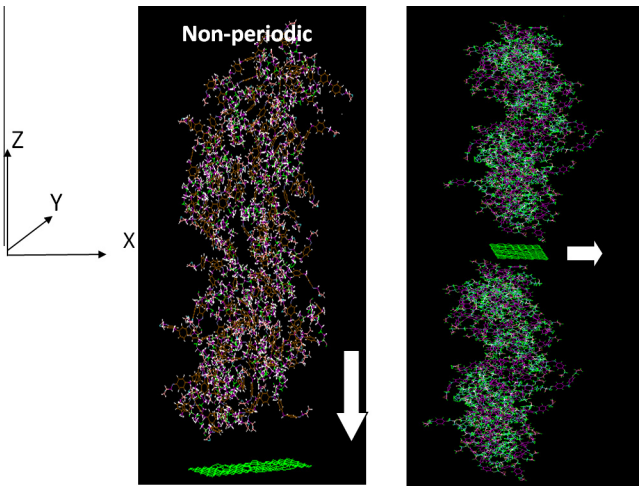

Fig. 3. Mode-I and Mode-II interface model of G–Ep system from epoxy.

and *x*-direction for normal and shear separations respectively. Details about unit cell configurations are provided in Table 3.

4. Computational details

MD equilibration was done prior to calculating mechanical properties. In this work three different categories such as amorphous, stacked graphene and interface models were considered. The following sections describe MD simulation scheme that was considered in each category. All the calculations were done using the open source molecular dynamics code LAMMPS [27].

4.1. Amorphous models

The initial stable configuration was obtained by minimizing the energy of each system by conjugate gradient method [23]. The average cutoff range for non-bonded interaction was 8 Å. All systems with type-a graphenes were subject to molecular dynamic equilibration under NVT (constant number of atoms, temperature and volume) condition with Nose–Hoover thermostat for 10,000 steps followed by NPT ensemble (constant number of atoms, pressure and temperature) for 5000 thousand steps at 300 K temperature and 0.0 atm external pressure. All the amorphous models with type-b graphenes were equilibrated under NVT for 30,000 steps at 300 K and NPT for 10,000 steps at 300 K temperature and 0.0 atm external pressure. Timestep size was 0.5–1.0 fs. Nose–Hoover barostat was used to add damping in the system [23]. Verlet time integration scheme was used throughout the simulation. Once the system is equilibrated, it underwent uniaxial deformation. At this stage, the amorphous systems were subjected to either uniaxial deformation in order to obtain stress–strain response using MD or series of deformations in all directions using MM in order to calculate Young's modulus and shear modulus. Within 1500 steps, the unitcells were subjected to 0.0001 engineering strain at every 300 steps under NVT ensemble at 0.1 K. After applying strains at each step, the running averaged stress throughout the unitcell was calculated [27]. Timestep size was 0.7–1.0 fs during deformation.

Molecular mechanics (MM) based deformation method requires a series of deformations in *xx–yy–zz–xy–yz–xz* directions. The velocity components of each atom were reset to zero prior to MM simulation. This was done in order to remove the effect of entropy. The equilibrated unitcells were subjected to $\pm 10^{-8}$ strain in all the directions. After each deformation spatially averaged stress throughout the system was calculated. The stiffness matrix components were calculated using Eq. (3).

Fig. 4 shows typical energy, temperature and pressure profiles with respect to time during MD equilibration process. These data were collected from the model G–Ep-Nc-IV during NVT and NPT based equilibration. Temperature and total energy profiles are obtained during NVT runs. It is noticed that, after 1500 fs the energy as well as temperature become very stable. The temperature is expected to converge approximately at 300 K as the temperature of the heat bath is 300 K. And the energy converges to 4.0×10^4 - kcal/mol for this specific system. This confirms that the system was properly equilibrated during NVT runs. According to the third plot in Fig. 4 the pressure in this system was observed to be stable around 0.0 atm during NPT runs.

4.2. Stacked graphene model

In the stacked graphene models the energy was minimized using conjugate gradient method followed by NVT based MD runs for 5000 steps at 300 K. Timestep size was 0.8–1.0 fs and the cutoff distance was 8 Å. The positions and velocities of the atoms were updated using verlet time integration scheme. Once the system is equilibrated, it was subjected to deform in *xx–yy–zz* directions. Within 1000 steps, each unit cell was deformed at every 100 under NVT at 0.1 K. The amount of applied strain was within the range of 0.0005–0.001. Nose–Hoover thermostat was used. The atoms in the systems were also subjected to damping term in every 100 fs. After each deformation, the running averaged stress was calculated using Eq. (1) to obtain stress–strain response.

4.3. Interface models

Both normal and shear separation forces were calculated on a slowly displaced graphene sheet in normal and shear directions as shown in Fig. 3. Such displacements lead to mode-I and mode-II separation. Initially, the space between epoxy and graphene sheet was maintained approximately 2 Å. The cutoff distance was 20 Å. For mode-I case, the graphene–epoxy unit cell is non-periodic in *z*-axis. Similarly, for mode-II case the system was nonperiodic in *xy* plane. The reaction forces on graphene due to mode-I or mode-II separation were calculated. This leads us to obtain forces vs. displacement curve for both mode-I and mode-II cases. The weight percentage of graphene was maintained higher than 3% in order to emphasize the effect of graphene on van der Waals interaction between epoxy and graphene. Prior to transverse or longitudinal movements of graphene plate, energy was minimized in all the systems using conjugate gradient method. Energy and force

Table 3
Unit cell configuration for interface model.

Configuration	Graphene sheet dimension (length × width) (Å)^2	Aspect ratio	Number of carbon atoms in graphene	Interaction force type
Mode-I-a	39.36 × 19.02	AR-LW ⩾ 2.06, AR-LT ⩾ 25.5	248	Normal
Mode-I-b	118.08 × 19.02	AR-LW ⩾ 6.20, AR-LT ⩾ 76.67	766	Normal
Mode-II-a	39.36 × 19.02	AR-LW ⩾ 2.06, AR-LT ⩾ 25.5	248	Shear
Mode-II-b	118.08 × 19.02	AR-LW ⩾ 6.20, AR-LT ⩾ 76.67	766	Shear

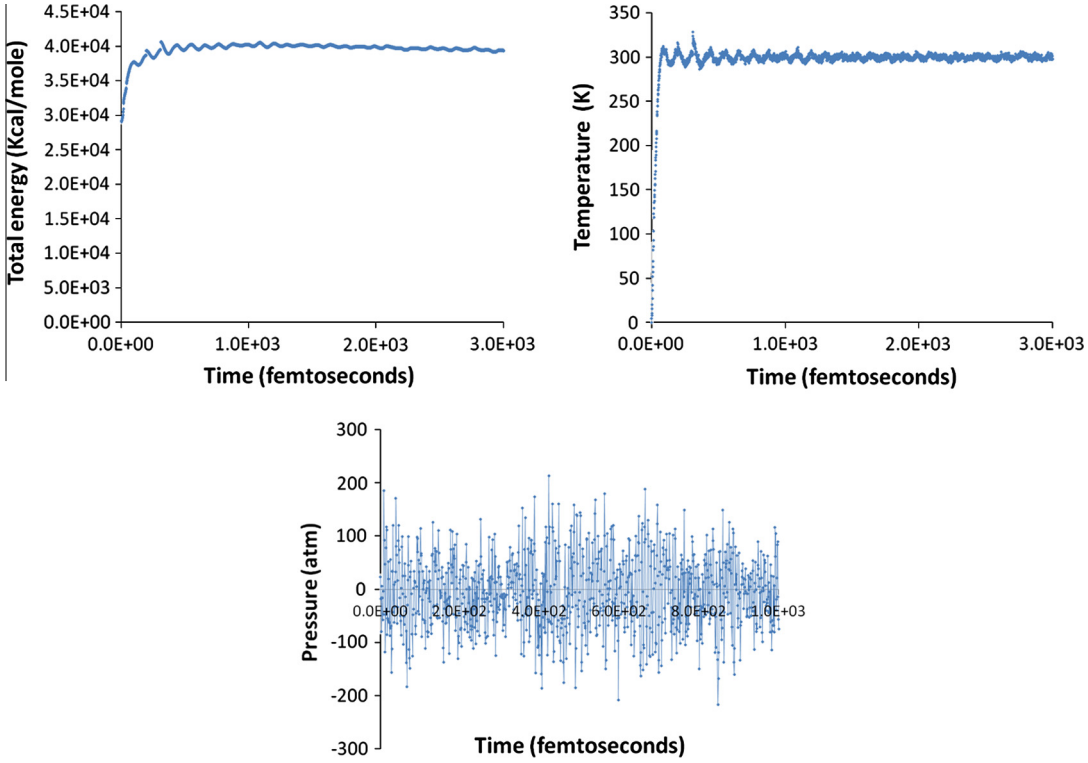

Fig. 4. Typical temperature, total energy and pressure plots at different times.

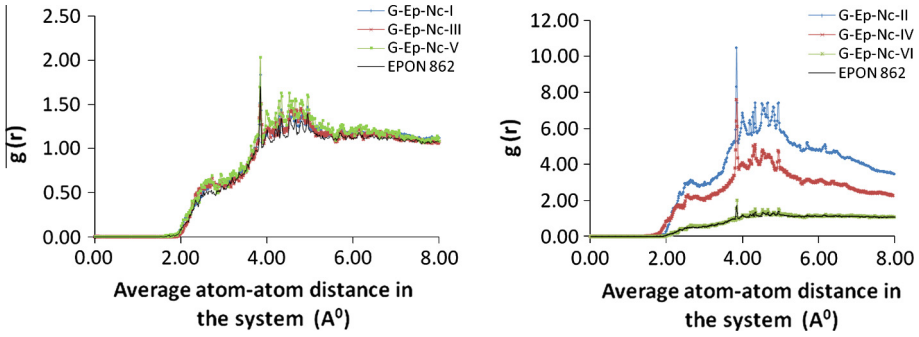

Fig. 5. RDF of any pair of atoms in graphene–epoxy amorphous system (Left: AR-LT 150 and Right: AR-LT 480).

tolerance were in the order of 10^{-10}. After the minimization, each system was equilibrated under NVT for 5000 steps with step size 1.0 fs. Once the systems are equilibrated, graphene was moved away from the polymer matrix by average translation rate of 0.01 Å/fs for 0.5–3.0 ps in transverse direction (pullout) and 0.001–0.0001 Å/fs for 1.5 ps in longitudinal direction (cohesive). The positions and velocities of the atoms were updated using verlet time integration scheme.

5. Results and discussion

The first part of this section focuses on analyzing radial distribution function (RDF), atom density and evolution in molecular energy of different G–Ep systems. This is important in understanding the characteristics of simulated molecular models. Later the effects of graphene aspect ratio, weight percentage and dispersion on elastic modulus of G–Ep nanocomposites are discussed. The interfacial properties such as cohesive force and pull out forces of G–Ep system are analyzed. Finally, the results obtained from this study are compared with the same determined using micromechanics model, nanoindentation test and coupon test data.

5.1. Radial distribution function (RDF)

In general, RDF $g(r)$ is a correlation function which relates the pairwise particle (atoms, molecules) density in a system to the distance from a reference point. As a result RDF provides information about the distribution pattern of particles such as graphene atoms and epoxy molecule in G–Ep system. Fig. 5 shows RDF of any pair of atoms in G–Ep system. The absence of any noticeable sharp peaks in the RDF ensures the amorphous nature of the graphene–epoxy system. The highest peak is observed at 3.9 Å which indicates maximum concentration of atoms in the entire system at this pairwise distance. The influence of graphene concentration is seen to be insignificant on RDF for type-a sample. But highest and lowest values of $g(r)$ are seen in type-b G–Ep system with 1% and 5% graphene concentrations, respectively. G–Ep systems lose any possibility of local order beyond pairwise distance of 6 Å.

5.2. Atom density

In molecular modeling atom density in the unit cell plays an important role in affecting mechanical properties. In all these unit

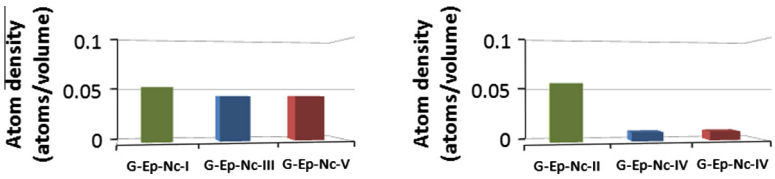

Fig. 6. Atom density in amorphous system (Left: AR-LT 150 and Right: AR-LT 480).

cells, number of epoxy molecules was changed in order to obtain necessary weight percentage of graphene. Thus, atom density in a unit cell is changed with respect to different weight percentage. Fig. 6 shows atom densities as a function of graphene concentrations in the unit cell for both type-a and type-b nanocomposites. The atom density in type-b G–Ep nanocomposites is significantly low for 3% and 5% graphene systems and corresponding Young's modulus is also seen to be significantly low as shown in Table 4. Highest atom density is observed in unit cells with 1% graphene content which also shows comparatively highest Young's and shear modulus. The RDF for type-b graphene system in Fig. 5 showed comparatively weaker pairwise correlation in the G–Ep systems with 5% graphene. This is possibly due to lower atom density in G–Ep-Nc-IV and G–Ep-Nc-V unit cells.

5.3. Molecular energy

The applied strain causes change in atom positions, velocities and overall molecular structure resulting an increase in overall potential energy. In general, potential energy consists of molecular energy $(E_{mol} = E_{Bond} + E_{Angle} + E_{Torsion} + E_{Dihedral} + E_{Cross\text{-}terms})$ and van der Waals energy [27]. The potential energy has comparatively larger contribution in total molecular energy than van der Waals energy. The change in molecular energy followed by applied deformation indicates the sensitivity of the molecules against applied strain. Fig. 7 shows molecular energy verses strain plots for G–Ep nanocomposites with graphene concentration 1%, 3% and 5% for both type-a and type-b graphenes. The increase in slope of molecular energy clearly explains the deformation in the molecular topology with applied strain. The molecular energy plot is seen to be comparatively steeper and higher for G–Ep with 1% graphene which provided higher stiffness. But the change in molecular energy is observed to be very small in G–Ep with 5% graphene showing comparatively lower modulus. It is to be noted that the amount of molecular energy is also seen to be higher with increased aspect ratio as seen in Fig. 7.

5.4. Effects of graphene concentrations and aspect ratio on elastic constants

The MD simulated stress–strain responses of G–Ep nanocomposites with graphene concentrations (1%, 3% and 5%) and aspect ratios (AR-LT: 150, 480, AR-LW: 5, 10) are shown in Fig. 8a. The values of Young's modulus (E) were determined from the slope of individual curve. In MM method, Young's modulus, E and shear modulus G, were calculated from Lame's constants λ, μ defined by Eq. (3). In Table 4, Young's modulus E and shear modulus G of G–Ep nanocomposites calculated by molecular mechanics (MM) and molecular dynamic (MD) methods are provided. The MM and MD simulation results are then compared with the data generated by Mori–Tanaka micromechanics (MTM) model [17]. The effects of graphene weight concentrations and aspect ratios on Young's modulus and shear modulus of G–Ep nanocomposites are shown in Table 4. Finally, these data are compared with neat epoxy resin. In Table 4, Young's modulus and shear modulus of neat epoxy resin (EPON 862) are seen to be 2.5 GPa and 0.95 GPa, respectively by MM simulation. But the MD simulation shows Young's modulus of neat epoxy resin equals to 3.42 GPa. The Young's modulus and shear modulus data of G–Ep nanocomposites predicted using MM, MD and MTM simulations are seen to be comparatively higher than those of neat epoxy resin. The Young's modulii for different G–Ep systems are seen to be in the range 1.34–4.56 GPa by MM and 1.77–5.0 GPa by MD simulations. It is observed that Young's modulus predicted by MD is comparatively higher than the same predicted by MM method. This trend is seen for both type-a and type-b samples. These variations are reasonable since the energy associated with atom's linear momentum is not incorporated in MM simulation. It is seen that modulus of nanocomposites with lower graphene concentration (1% by weight) is comparatively higher than the same with higher concentration (5% by weight). This is possibly due to the variation in atom density. The results show comparatively higher E value with decreased aspect ratio in comparison to increased aspect ratio. In

Table 4
Effect of graphene concentrations and aspect ratio on elastic constants.

Material configuration	Aspect ratio (AR)	Weight percentage of graphene (%)	Young's modulus (MM): E (Gpa)	Shear modulus (MM): G (Gpa)	Young's modulus from stress–strain (MD) response (GPa)	Young's modulus from micromechanics (MTM) model (GPa) [17]
G–Ep-Nc-I	AR-LW $\geqslant$ 5, AR-LT $\geqslant$ 150 (Type-a)	1	4.56	1.73	5.00	2.96
G–Ep-Nc-II	AR-LW $\geqslant$ 10, AR-LT $\geqslant$ 480 (Type-b)	1	3.45	1.16	4.27	2.63
G–Ep-Nc-III	AR-LW $\geqslant$ 5, AR-LT $\geqslant$ 150 (Type-a)	3	3.98	1.37	3.98	3.6
G–Ep-Nc-IV	AR-LW $\geqslant$ 10, AR-LT $\geqslant$ 480 (Type-b)	3	1.16	0.391	2.04	2.71
G–Ep-Nc-V	AR-LW $\geqslant$ 5, AR-LT $\geqslant$ 150 (Type-a)	5	2.98	1.07	3.56	4.33
G–Ep-Nc-VI	AR-LW $\geqslant$ 10, AR-LT $\geqslant$ 480 (Type-b)	5	1.34	0.45	1.77	4.69
EPON-862	Current work Literature value [12]		2.5 3.362	0.95 1.22	3.42 3.362	

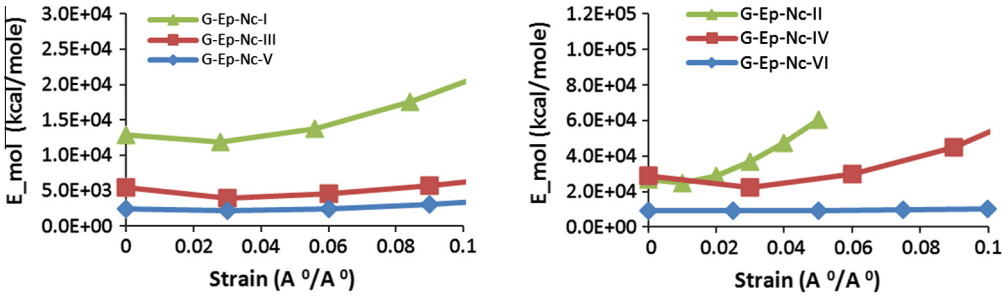

Fig. 7. Molecular energy in amorphous systems with type-a and type-b graphenes.

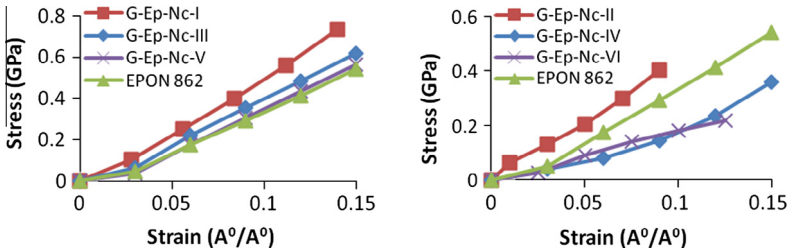

Fig. 8a. Stress–strain response of amorphous system with type-a and type-b graphenes.

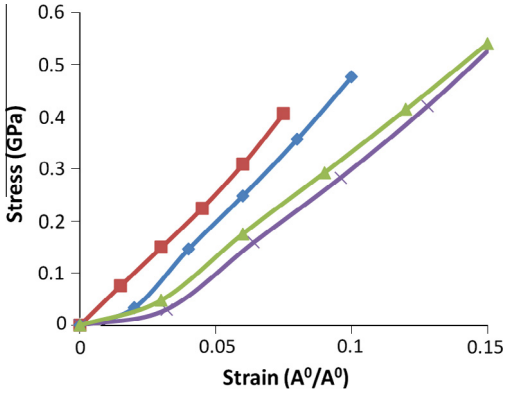

Fig. 8b. Stress–strain response of amorphous system with type-a^0.

Table 4, shear modulus, G is observed to be in the range of 0.45–1.73 GPa for G–Ep nanocomposites (type-a) in comparison to 0.95 GPa for neat epoxy resin. The results of this study show highest G (1.37 GPa) with lowest graphene concentration (1%) and lowest aspect ratio (150). The Young's modulus calculated using Mori Tanaka micromechanics (MTM) model show comparatively lower values in G–Ep system with 1% and 3% by weight concentration of graphene compared to MD simulation data. It is to be noted that the Young's modulus calculated by MTM method shows higher values with increased graphene concentrations but in MD simulation the similar trend is not observed. The micromechanics model assumes the unit cell as homogeneous. Hence, the prediction shows a monotonically increasing nature in Young's modulus with the increasing volume fraction of nanofiller. But in atomistic models, spatially distribution of atoms, atom density and change in molecular energy, etc. in the system play an important rule. Hence, monotonically increasing Young's modulus with respect to weight percentage of graphenes may not be realistic in actual scenario. Work by Rafiee et al. [6] showed initially increase and eventually decrease in the Young's modulus of graphene–epoxy nanocomposites as the weight percentage of graphene increases. They considered graphene sheet with length to width aspect ratio of 19 (approximately).

The in-house characterization of G–Ep nanocomposites using nanoindentation tests with 100 nm diameter Berkovich tip showed Young's modulus of 6.58 ± 1.33 GPa, 5.68 ± 1.81 GPa, 5.54 ± 1.25 GPa and 5.38 ± 0.80 GPa for the nanocomposites with 1%, 3%, 5% graphene and neat epoxy samples, respectively. The coupon test of the same specimens showed Young's modulus value approximately 2.17 GPa, 2.50 GPa, 2.07 GPa and 2.12 GPa, respectively. While comparing nanoindentation and coupon test data, it is observed that macroscopic values of Young's modulus are relatively lower than nanoindentation test data. Similar trend was also observed while comparing MD simulation results with micromechanics based MTM method. The Young's modulii from nanoindentation test are in reasonable agreement with MD simulation (Table 4). The Young's modulii are seen to be decreased with increased weight concentration of graphenes.

From the MD simulation and experimental data it is observed that the effects of graphene's aspect ratio as well as weight concentration on elastic properties are significant. Graphenes with lower length to width ratio (i.e. type-a) seem to be better in enhancing stiffness of the G–Ep nanocomposites. From Table 4 it is observed that Young's modulus and shear modulus are decreased when graphene with larger aspect ratio was used. The Young's modulus is decreased by 14% (approximately) for 1% weight concentration. This becomes 50% (approximately) for 5% graphene weight concentration. So at larger weight concentration of graphene the effect of aspect ratio becomes more significant. In order to get a better picture a third aspect ratio of graphene was considered. The length to width aspect ratio AR-LW = 2 (approximately) was considered. This was done by increasing the width of type-a graphene by approximately 2.14 times. Hence the AR-LT becomes 20 (approximately). Let us name this graphene as type-a^0. The G–Ep systems were built and equilibrated using type-a^0 graphene with 1%, 3% and 5% weight concentrations. As shown in Fig. 8b, the stress–strain responses were obtained from the MD simulation. The calculated Young's modulii for 1%, 3% and 5% type-a^0 graphene are 5.23 GPa, 4.44 GPa and 3.27 GPa, respectively. For 1% and 3% weight concentrations, the Young's is higher in type-a^0 graphene based systems compared

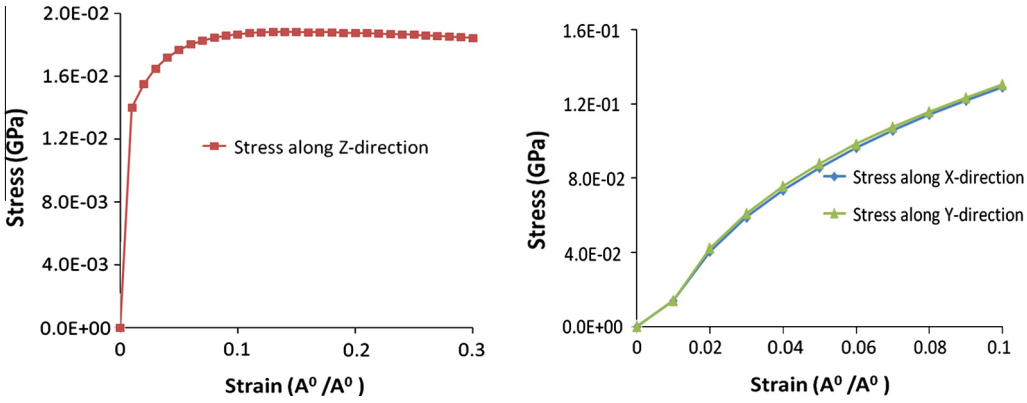

Fig. 9. Stress–strain response in *xx*, *yy* and *zz* directions for SGM-GnEp-I.

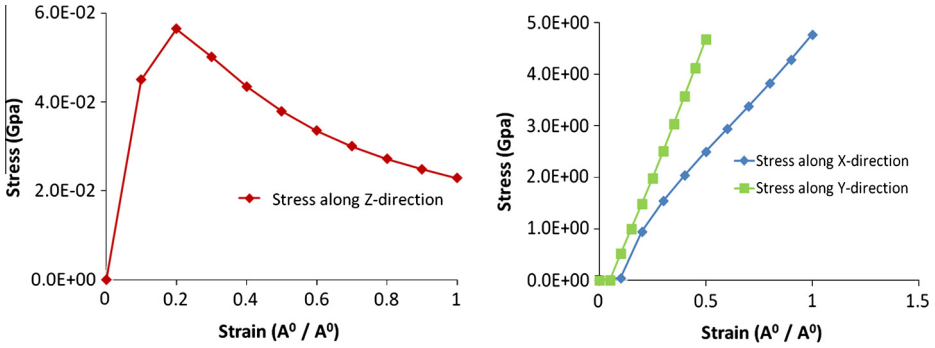

Fig. 10. Stress–strain response in *xx*, *yy* and *zz* directions for SGM-GnEp-II.

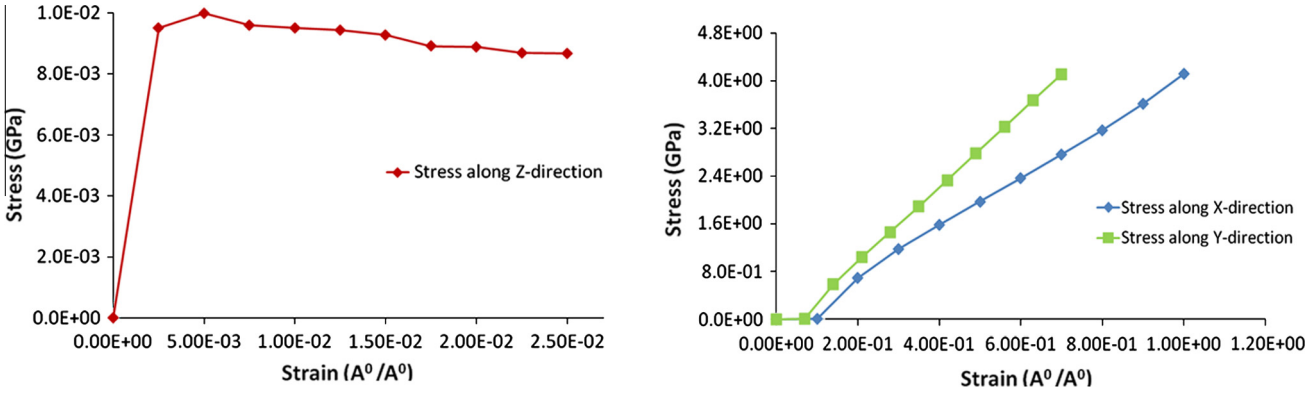

Fig. 11. Stress–strain response in *xx*, *yy* and *zz* directions for SGM-GnEp-III.

to type-a and type-b graphene systems. However, for 5% weight concentration, the type-a^0 graphene seems to reduce the Young's modulus. Hence, it can be concluded that the smaller length to width ratio leads to better stiffness at low graphene content.

5.5. Dispersion and agglomeration effects

Figs. 9–11 show MD simulated stress–strain responses in *x*, *y* and *z* directions of single, dispersed and agglomerated G–Ep models shown earlier in Fig. 2. In this case, *x* and *y* represent graphene length and width direction and *z* corresponds to thickness direction. The strain was applied independently in *x*, *y* and *z* direction. It is seen that stress generated in *z* direction is significantly low compared to *x* and *y* direction for all three cases. This occurs since stress in thickness direction is mostly matrix dominant whereas in-plane properties are dominated by stronger reinforcing graphene. The variations in stress–strain responses in *x* and *y* direction as seen in Figs. 9 and 10 are mostly due to different graphene length to width ratio and variable cell size used in these models. The stress–strain plots in *z*-directions shown in Figs. 10 and 11 indicate that at a typical design strain (4%), the stiffness of dispersed system is comparatively lower than the same in agglomerated system.

Table 5 shows Young's modulus of single, dispersed and agglomerated graphene system calculated from stress–strain

Table 5
Young's modulus calculated from stress–strain response for stacked graphene model.

Configuration	Number of graphene plates	E_x (GPa)	E_y (GPa)	E_z (GPa)
SGM-GnEp-I	1	1.89	1.94	0.9
SGM-GnEp-II	3 (dispersed)	4.81	8.76	0.32
SGM-GnEp-III	3 (agglomerated)	3.99	5.67	2.36

responses in x, y and z directions. It is evident that in plane Young's modulus, E_x and E_y for the dispersed system (4.81 GPa, 8.76 GPa) is comparatively higher than the same in agglomerated system (3.99 GPa, 5.67 GPa). It is to be noted that higher modulus was observed in graphene width direction rather than length direction. As a result well dispersed graphene with high aspect ratio is seen to provide improved in-plane Young's modulus. It is also seen that in-plane modulus in three graphene system is comparatively larger than single graphene system. This indicates that in-plane modulus is significantly influenced by graphene's volume fraction since graphene's in-plane property is significantly high (Young's modulus, 1 TPa). However, the out of plane Young's modulus, E_z of the G–Ep nanocomposites is mostly controlled by stiffness of epoxy and non-bonded interaction (van der Waals) between graphene–epoxy or graphene–graphene. The results show lowest E_z value (0.32 GPa) for three layer dispersed graphene system. The highest E_z value (2.36 GPa) was provided by three layer agglomerated system. The single layer graphene system shows E_z equals to 0.9 GPa. In agglomerated system, van der Walls interaction between graphene–graphene molecules possibly results such increased Young's modulus.

5.6. Interfacial property

Interface between graphene and epoxy plays a significant role in load transfer mechanism between graphene and epoxy. The normal and shear displacement at the interface under applied strain have been investigated. Normal displacement of graphene leads us to understand cohesive traction-separation mechanism between graphene and epoxy whereas shear displacement provides information about the pullout mechanism. The unit cell configurations and relevant interface models under normal and shear displacements are shown in Table 3 and Fig. 3. As MD simulation was conducted under displacement control, a reaction force was developed on the graphene sheet. Fig. 12 shows normal force verses displacement plots at the interface under mode-I separation for both type-a (AR-25.5) and type-b (AR-76.67) graphene plates. The trend of the force–displacement plot under mode-I is seen to be linear at the initial stage. It shows some nonlinearity before reaching to a peak point. The cohesive force then gradually drops to zero with increased displacement. In Fig. 12, the maximum cohesive force and the displacement for Mode-I-a case are seen to be 80 pN and 1.6×10^{-4} nm but the same are observed to be

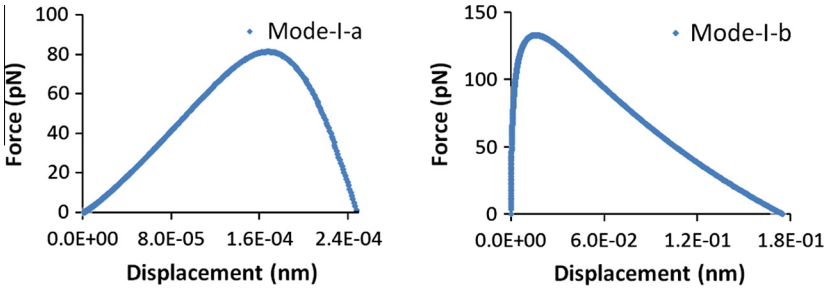

Fig. 12. Force vs displacement curve for Mode-II-b graphene–epoxy system.

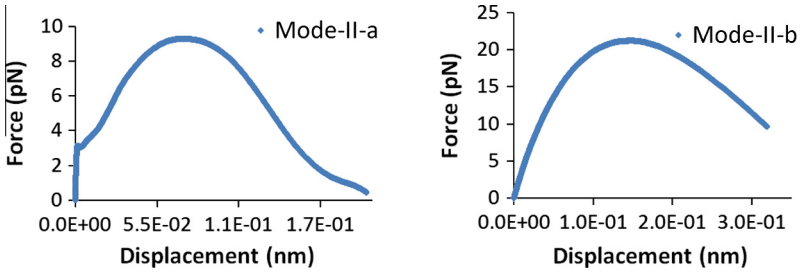

Fig. 13. Force vs displacement curve for Mode-I-a graphene–epoxy system.

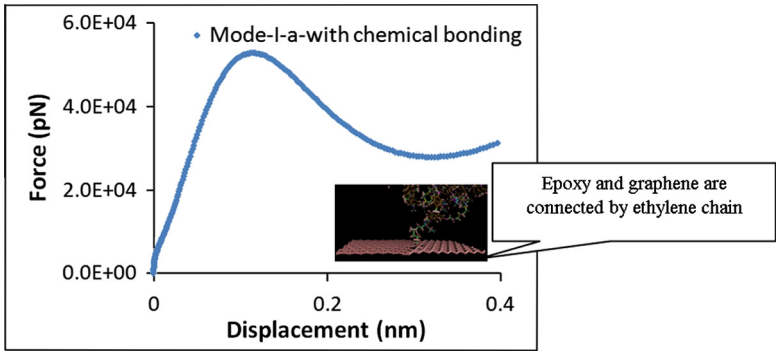

Fig. 14. Force vs displacement curve for Mode-I-a-with chemical bonding system.

130 pN and 1.6×10^{-2} nm for Mode-I-b. As a result the cohesive force is seen to be enhanced with increased aspect ratio of the graphene sheet. In this study, the magnitude of the cohesive force is seen to be very small which mostly resulted from van der Walls force interaction between graphene and epoxy. Such cohesive force may be increased by minimizing the gap between graphene and epoxy or introducing a covalent bond between graphene and epoxy.

In Fig. 13, shear force verses displacement plots are shown under pullout separation mode for both type-a (AR-25.5) and type-b (AR-76.67) graphene system. In Fig. 13 the maximum pullout force is observed to be 9 pN at a displacement of 0.05 nm for Mode-II-a. The same is seen to be 22 pN at a displacement of 0.15 nm for Mode-II-b. The maximum pullout force is also seen to be increased with increased graphene aspect ratio due to enhanced interfacial surface area. It is obvious that maximum pullout force under shear separation mode is significantly low compared to maximum cohesive force under normal separation mode. It is to be noted that interfacial properties were entirely dependent on the van der Waals interactions. This leads to comparatively weaker interfacial property. Thus in order to improve the interfacial properties chemical bonding was introduced between graphene and epoxy as shown in Fig. 14. An ethylene chain was introduced as a connecting interface between graphene and carbon atom in epoxy. Fig. 14 shows force vs. displacement plots of chemically bonded graphene epoxy system. The result shows significantly increased cohesive force of 40,000 pN compared to 80 pN for chemically functionalized graphene. This suggests for functionalization of graphenes in order to improve interfacial as well as elastic properties of graphene–epoxy nanocomposites. Along the similar direction, Yang et al. [28] performed similar study with nanosilica reinforced polyimide nanocomposites. They used propyl as a functionalizing group to create chemical bonding between polyimide and nanosilica particle. Their study showed that the interfacial as well as elastic properties can be significantly (more than 20%) improved by introducing such functionalization. Hence introduction of such chemical functionalization seems to be promising for G–Ep nanocomposites. However, the detail study on this issue is beyond the scope of this paper. This will be addressed in the future work.

6. Conclusion

A molecular modeling frame work has been developed in order to determine Young's modulus, shear modulus and interfacial properties such as cohesive force and pullout force of graphene/epoxy nanocomposites. The effects of graphene weight concentrations, dispersion and aspect ratio have also been studied. The molecular energy, molecular density and radial density functions (RDF) have been analyzed for simulated models. The following conclusions are drawn from this investigation.

i. The RDF of G–Ep system indicates that maximum concentration of epoxy molecules and graphene atoms is observed at an approximate pairwise separation distance 4 Å. The presence of any atoms and molecules was not observed within a distance of 2 Å due to repulsive force.
ii. The slope of molecular energy verses strain plots indicates progressive deformation in G–Ep system during MD simulation. The strength and elastic modulus of G–Ep nanocomposites are seen to be increased due to enhanced slope of molecular energy verses strain plots.
iii. The atom density in MD model influences performance of G–Ep system. The Young's modulus is seen to be increased with enhanced atom density in MD model.
iv. The RDF, molecular energy and atomic density of G–Ep system are influenced by graphene concentration and aspect ratios. High aspect ratio and graphene concentrations in the range 1–3% are observed to increase RDF, molecular energy and atomic density in G–Ep system.
v. The Young's modulus and shear modulus data of G–Ep nanocomposites are seen to be comparatively 25–40% higher than those of neat epoxy resin. The graphene concentrations in the range of 1–3% and graphene with lower aspect ratio provided improved Young's modulus. The Young's modulus determined by molecular modeling and nanoindentation tests are seen to be comparatively higher than the same obtained by micromechanics computations and coupon tests which is probably due to scaling effects.
vi. It is observed that dispersed graphene with high aspect ratio provides improved in-plane Young's modulus of G–Ep in comparison to agglomerated graphene system. The out of plane modulus in aligned (unidirectional) G–Ep system is significantly low compared to in plane modulus in x and y direction.
vii. The maximum cohesive force and pullout force are seen to be increased with increased graphene aspect ratio. It is noticed that attachment of chemical bond at the interface significantly enhances cohesive force. This suggests functionalization of graphene for improved interfacial properties of G–Ep nanocomposites.

Acknowledgement

The work is supported by NSF EPSCoR Research Grant #23669.

References

[1] Hossain F, Dean D, Haque A, Shamsuzzoha M. S2 glass/vinyl ester polymer nanocomposites: manufacturing, structures, thermal and mechanical properties. J Adv Mater 2005;37(1):16–27.
[2] Haque A, Shamsuzzoha M, Hossain F, Dean D. S2-glass/epoxy nanocomposites: manufacturing, structures, thermal and mechanical properties. J Compos Mater 2003;37:1821–37.
[3] An LN, Xu WX, Rajagopalan S, Wang CM, Wang H, Fan Y, et al. Carbon-nanotube-reinforced polymer-derived ceramic composites. Adv Mater 2004;16(22):2036–40.
[4] Yasmin A, Daniel IM. Mechanical and thermal properties of graphite/epoxy composites. Polymer 2004;45:8211–9.
[5] Cho J, Luo JJ, Daniel IM. Mechanical characterization of graphite/epoxy nanocomposites by multi-scale analysis. Compos Sci Technol 2007;67:2399–407.
[6] Rafiee MA, Rafiee J, Wang Z, Song H, Yu ZZ, Koratkar N. Enhanced mechanical properties of nanocomposites at low graphene content. ACS Nanolett 2009;3(12):3884–90.
[7] Haque A, Ramasetty A. Theoretical study of stress transfer in carbon nanotube reinforced polymer matrix composites. Compos Struct 2005;71:68–77.
[8] Zhu R, Pan E, Roy AK. Molecular dynamics study of the stress–strain behavior of carbon-nanotube Epon 862 composites. Mater Sci Eng A 2007;447:51–7.
[9] Wu C, Xu W. Atomistic molecular modeling of crosslinked epoxy resin. Polymer 2006;47:6004–9.
[10] Fan HB, Yuen MMF. Material properties of the cross-linked epoxy resin compound predicted by molecular dynamics simulation. Polymer 2007;48:2174–8.
[11] Bandyopadhay A, Jensen D, Valavala KP, Odegard MG. Atomistic modeling of cross-linked epoxy polymer, in: Presented at 51st AIAA/ASME/ASCE/ASC Structures, Structural Dynamics and Materials Conference 12–15th April, 2010.
[12] Suyoung Y, Seunghwa Y, Cho M. Multi-scale modeling of cross-linked epoxy nanocomposites. Polymer 2009;50:945–52.
[13] Franklans SJV, Harik VM, Odegard GM, Brenner DW, Gates TS. The stress–strain behavior of polymer–nanotube composites from molecular dynamics simulation. Compos Sci Technol 2003;63:1655–61.
[14] Choi J, Yang S, Yu S, Shin H, Cho M. Method of scale-bridging for thermoelasticity of cross-linked epoxy/SiC nanocomposites at a wide range of temperatures. Polymer 2012;53:5178–89.
[15] Yang S, Yu S, Cho M. Sequential thermoelastic multiscale analysis of nanoparticulate composites. J Appl Phys 2010;108:056102.
[16] Yang S, Cho M. Scale bridging method to characterize mechanical properties of nanoparticle/polymer nanocomposites. Appl Phys Lett 2008;93(4):043111.

[17] Xiang YJ, Cao YP, Feng XQ. Micromechanics prediction of the effective elastic moduli of graphene sheet-reinforced polymer nanocomposites. Model Simulat Mater Sci Eng 2010;16:45005–20.
[18] Cheng Lv, Qingzhongx Q, Ma M, Xia D. Effect of chemisorption structure on the interfacial bonding characteristics of graphene–polymer composites. Appl Surf Sci 2011;258(6):2077–82.
[19] Kin L, Li S. Interfacial characteristics of a carbon nanotube–polystyrene composite system. Appl Phys Lett 2001;79:4225–7.
[20] Awasthi AP, Lagoudas DC, Hammerand DC. Modeling of graphene–polymer interfacial mechanical behavior using molecular dynamics. Model Simulat Mater Sci Eng 2009;17(1):015002.
[21] Sun H. Compass: an ab initio force field optimized for condensed phase applications overview with details on alken and benzene compounds. J Phys Chem B 1998;102(38):7338–64.
[22] Feng CF, Ling SH. Application of the molecular simulation technique to characterize the structure and properties of an aromatic polysulfone system. Mechanical and thermal properties. Macromolecules 1992;25:266–70.
[23] Leach AR. Molecular modelling: principles and applications. Addison Wesley Publishing Company; 1997.
[24] Shenogin S, Ozisik R. Xenoview: visualization for atomistic simulations; 2007. <http://xenoview.mat.rpi.edu/>.
[25] Sakhaee AP. Elastic properties of single layered graphene sheet. Solid State Commun 2009;149:91–5.
[26] Dubois SM-M, Zanolli Z, Declerck X, Charlier J-C. Electronic properties and quantum transport in graphene-based nanostructures. Eur Phys J B 2009;71(1):1–24.
[27] Plimpton S, Fast Parallel Algorithms for Short-Range Molecular Dynamics, J Comp Phys, 117, 1995, 1-19. http://lammps.sandia.gov/.
[28] Yang S, Choi J, Cho M. Elastic stiffness and filler size effect of covalently grafted nanosilica polyimide composites: molecular dynamics study. Appl Mater Interf 2012;4(9):4792–9.